Proceedings of the World Congress on Engineering 2010 Vol III
WCE 2010, June 30 - July 2, 2010, London, U.K.

Biharmonic Computation of the Flow Past an Impulsively Started Circular Cylinder at $Re = 200$

Jiten C Kalita * Shuvam Sen †

Abstract—**In this paper, we apply a second order temporally and spatially accurate finite difference scheme for biharmonic form of the transient incompressible 2D Navier-Stokes (N-S) equations on irregular geometries to simulate viscous flow past an impulsively started circular cylinder for Reynolds number (Re) 200. We have studied time evolution of flow structure and validate our results with established numerical and experimental observations available in the literature; excellent comparison is obtained in all the cases.**

Keywords: biharmonic, circular cylinder

1 Introduction

Flow over a bluff body is a common occurrence. It occurs with fluid flowing over an obstacle or with the movement of a natural or artificial body. Common examples are the flows past an airplane, a submarine, an automobile, or wind blowing past a high-rise building. Although many different shapes of bluff bodies exist, the circular cylinder is considered to the representative two dimensional bluff body. As such the flow around a circular cylinder has been the subject of intense research in the last century and numerous theoretical, numerical and experimental investigations have been reported in the literature [1, 2, 3, 4, 5, 6, 7, 8, 9, 10, 11]. The time development of an incompressible viscous flow induced by an impulsively started circular cylinder is now a classical problem in fluid mechanics. It displays almost all the fluid mechanical phenomena for incompressible viscous flows in the simplest of geometric settings.

In experiment, it is difficult to study the transition from an initially steady flow to the final periodic vortex shedding flow in detail. On the other hand, in numerical simulation all aspects of the flow for every stage of the flow development remain available. Our focus here is to examine through numerical simulation the development of periodic vortex shedding as well as initial laminar flow profile as the oncoming flow velocity is increased from zero to a terminal value. This corresponds of course to the situation when a body is accelerated from rest to a certain speed. Some of the experimental and numerical works that may be cited which have studied this flow regime including the phenomenon of vortex shedding are [8, 10, 12, 13, 14, 15, 16, 17].

Over the years, the CFD community has seen the extensive use of both the primitive variable and streamfunction-vorticity (ψ-ω) formulation to compute incompressible viscous flows governed by the N-S equations. Both these formulations have their relative advantages and disadvantages over each other: while the primitive variable formulation has been traditionally difficult because of the presence of pressure term in the governing equations, a typical difficulty with the ψ-ω formulation is that the vorticity ω is not prescribed on the boundaries. Considering these facts, the ψ-v formulation that uses the biharmonic form of the N-S equations has emerged as an attractive alternative approach of solving the N-S equation. This approach [18, 19, 20, 21, 22, 23] eliminates the need to compute pressure and vorticity as a part of the computational process and therefore computationally much faster than the primitive variable and ψ-ω formulations.

However, the use of all these schemes developed for the biharmonic form of the N-S equations were limited to uniform grids only, that too, in simple rectangular geometries. In the present study, we apply a recently proposed compact scheme [24] which is second order accurate in both space and time for the transient N-S equations on non-uniform grids capable of tackling geometries beyond rectangular. The grid is constructed using a conformal mapping, which results in a general orthogonal grid, where the degree and nature of the non-uniformity can be specified to meet the needs of the problem being studied. Further, using the compact approach we discretize this biharmonic equation using unknown solution ψ and its gradients ψ_x and ψ_y at interior grid points.

Our main focus in this paper is to analyze the flow past an impulsively started circular cylinder in the laminar

*Department of Mathematics, Indian Institute of Technology Guwahati, Guwahati 781039, Assam, INDIA, Email: jiten@iitg.ernet.in, the author is thankful to the Department of Science and Technology, Government of India for supporting a part of the work by providing financial support in the form of a project (Project No. SR/S4/MS: 468/07).

†Department of Mathematical Sciences, Tezpur University, Tezpur 784028, Assam, INDIA, Email: shuvam@tezu.ernet.in, the author is thankful to the University Grants Commission (UGC), Government of India for supporting a part of the work by providing financial support in the form of a minor project (Project No. F. No. 37-537/2009(SR)).

ISBN: 978-988-18210-8-9
ISSN: 2078-0958 (Print); ISSN: 2078-0966 (Online)

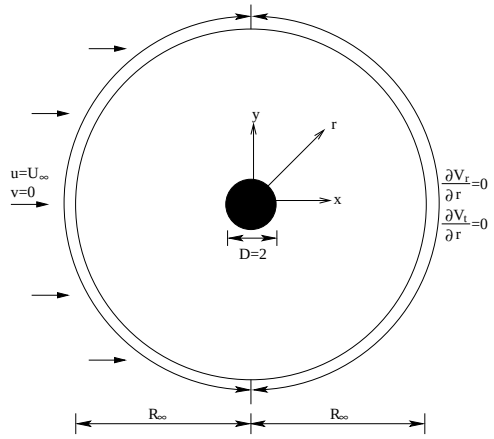

Figure 1: Configuration of the flow past a circular cylinder problem.

flow regime where the flow eventually becomes periodic. In this simulation we have studied time evolution of flow structure for Reynolds number $Re = 200$. We have compared our results both qualitatively and quantitatively with established numerical and experimental results and excellent comparison is obtained in all the cases.

2 The Problem

The problem is that of the laminar flow past a circular cylinder placed in a channel of infinite length. The flow is governed by the incompressible Navier-Stokes (N-S) equations which in primitive variables in non-dimensional (details are given in [24]) form are given by

$$\frac{\partial u}{\partial x} + \frac{\partial v}{\partial y} = 0 \tag{1}$$

$$\frac{1}{2}\frac{\partial u}{\partial t} + u\frac{\partial u}{\partial x} + v\frac{\partial u}{\partial y} = -\frac{\partial p}{\partial x} + \frac{2}{Re}\left(\frac{\partial^2 u}{\partial x^2} + \frac{\partial^2 u}{\partial y^2}\right) \tag{2}$$

$$\frac{1}{2}\frac{\partial v}{\partial t} + u\frac{\partial v}{\partial x} + v\frac{\partial v}{\partial y} = -\frac{\partial p}{\partial y} + \frac{2}{Re}\left(\frac{\partial^2 v}{\partial x^2} + \frac{\partial^2 v}{\partial y^2}\right) \tag{3}$$

where t is the time, u, v are velocities along the x- and y-directions respectively, p represents the pressure and Re is the non-dimensional Reynolds number. The problem configuration is as shown in Figure 1.

2.1 The Numerical Scheme

To simulate the flow, we have used the recently developed compact scheme for biharmonic formulation for the transient N-S equations by Kalita and Sen [24]. Making use of the fact that the velocities u and v are defined in terms of the streamfunction ψ as $u = \psi_y$ and $v = -\psi_x$ and considering conformal transformation $x = x(\xi, \eta)$, $y = y(\xi, \eta)$ of the physical plane into a rectangular computational plane, the biharmonic form of transient N-S equation in terms of ψ is given as

$$\begin{aligned}\frac{JRe}{2}\frac{\partial}{\partial t}\nabla^2\psi &= \nabla^4\psi - (2C + \frac{Re}{2}\psi_\eta)\frac{\partial}{\partial \xi}\nabla^2\psi \\ &- (2D - \frac{Re}{2}\psi_\xi)\frac{\partial}{\partial \eta}\nabla^2\psi \\ &+ (E + C\frac{Re}{2}\psi_\eta - D\frac{Re}{2}\psi_\xi)\nabla^2\psi \end{aligned} \tag{4}$$

where $C = J_\xi/J,\ D = J_\eta/J,\ E = 2C^2 + 2D^2 - J_{\eta\eta}/J - J_{\xi\xi}/J$, J being the jacobian of the conformal transformation.

Equation (4) is discretized by the proposed extension that uses values of ψ and its gradients ψ_ξ, ψ_η in the compact square cell.

The finite difference approximation for (4) is given by

$$\begin{aligned}
&Re\frac{\pi^2 e^{2\pi\xi_i}}{8}h^2\big[\psi^{(n+1)}_{i+1,j} + \psi^{(n+1)}_{i-1,j} - 4\psi^{(n+1)}_{i,j} + \psi^{(n+1)}_{i,j+1} \\
&\qquad +\psi^{(n+1)}_{i,j-1}\big] \\
&= Re\frac{\pi^2 e^{2\pi\xi_i}}{8}h^2\big[\psi^{(n)}_{i+1,j} + \psi^{(n)}_{i-1,j} - 4\psi^{(n)}_{i,j} + \psi^{(n)}_{i,j+1} \\
&\qquad +\psi^{(n)}_{i,j-1}\big] + \delta t(1-\lambda) \\
&\Big[28\psi^{(n)}_{i,j} - 8(\psi^{(n)}_{i+1,j} + \psi^{(n)}_{i,j+1} + \psi^{(n)}_{i-1,j} + \psi^{(n)}_{i,j-1}) \\
&+(\psi^{(n)}_{i+1,j+1} + \psi^{(n)}_{i-1,j+1} + \psi^{(n)}_{i+1,j-1} + \psi^{(n)}_{i-1,j-1}) \\
&+3h(\psi^{(n)}_{\xi_{i+1,j}} - \psi^{(n)}_{\xi i-1,j} + \psi^{(n)}_{\eta_{i,j+1}} - \psi^{(n)}_{\eta_{i,j-1}}) \\
&-2\pi h^2\big(\psi^{(n)}_{\xi_{i+1,j}} + \psi^{(n)}_{\xi_{i-1,j}} - 4\psi^{(n)}_{\xi_{i,j}} + \psi^{(n)}_{\xi_{i,j+1}} + \psi^{(n)}_{\xi_{i,j-1}}\big) \\
&+\frac{Re}{4}h^2\Big(\psi^{(n)}_{\xi_{i,j}}\big(\psi^{(n)}_{\eta_{i+1,j}} + \psi^{(n)}_{\eta_{i-1,j}} + \psi^{(n)}_{\eta_{i,j+1}} + \psi^{(n)}_{\eta_{i,j-1}}\big) \\
&-\psi^{(n)}_{\eta_{i,j}}\big(\psi^{(n)}_{\xi_{i+1,j}} + \psi^{(n)}_{\xi_{i-1,j}} + \psi^{(n)}_{\xi_{i,j+1}} + \psi^{(n)}_{\xi_{i,j-1}}\big)\Big) \\
&+h^2\big(2\pi^2 + \frac{Re}{2}\pi\psi^{(n)}_{\eta_{i,j}}\big) \\
&\big(\psi^{(n)}_{i+1,j} + \psi^{(n)}_{i-1,j} - 4\psi^{(n)}_{i,j} + \psi^{(n)}_{i,j+1} + \psi^{(n)}_{i,j-1}\big)\Big] \\
&+\delta t\lambda\Big[28\psi^{(n+1)}_{i,j} - 8(\psi^{(n+1)}_{i+1,j} + \psi^{(n+1)}_{i,j+1} + \psi^{(n+1)}_{i-1,j} + \psi^{(n+1)}_{i,j-1}) \\
&+(\psi^{(n+1)}_{i+1,j+1} + \psi^{(n+1)}_{i-1,j+1} + \psi^{(n+1)}_{i+1,j-1} + \psi^{(n+1)}_{i-1,j-1}) \\
&+3h(\psi^{(n+1)}_{\xi_{i+1,j}} - \psi^{(n+1)}_{\xi i-1,j} + \psi^{(n+1)}_{\eta_{i,j+1}} - \psi^{(n+1)}_{\eta_{i,j-1}}) \\
&-2\pi h^2\big(\psi^{(n+1)}_{\xi_{i+1,j}} + \psi^{(n+1)}_{\xi_{i-1,j}} - 4\psi^{(n+1)}_{\xi_{i,j}} + \psi^{(n+1)}_{\xi_{i,j+1}} + \psi^{(n+1)}_{\xi_{i,j-1}}\big) \\
&+\frac{Re}{4}h^2\Big(\psi^{(n+1)}_{\xi_{i,j}}\big(\psi^{(n+1)}_{\eta_{i+1,j}} + \psi^{(n+1)}_{\eta_{i-1,j}} + \psi^{(n+1)}_{\eta_{i,j+1}} + \psi^{(n+1)}_{\eta_{i,j-1}}\big) \\
&-\psi^{(n+1)}_{\eta_{i,j}}\big(\psi^{(n+1)}_{\xi_{i+1,j}} + \psi^{(n+1)}_{\xi_{i-1,j}} + \psi^{(n+1)}_{\xi_{i,j+1}} + \psi^{(n+1)}_{\xi_{i,j-1}}\big)\Big) \\
&+h^2\big(2\pi^2 + \frac{Re}{2}\pi\psi^{(n+1)}_{\eta_{i,j}}\big) \\
&\big(\psi^{(n+1)}_{i+1,j} + \psi^{(n+1)}_{i-1,j} - 4\psi^{(n+1)}_{i,j} + \psi^{(n+1)}_{i,j+1} + \psi^{(n+1)}_{i,j-1}\big)\Big]
\end{aligned} \tag{5}$$

ISBN: 978-988-18210-8-9
ISSN: 2078-0958 (Print); ISSN: 2078-0966 (Online)

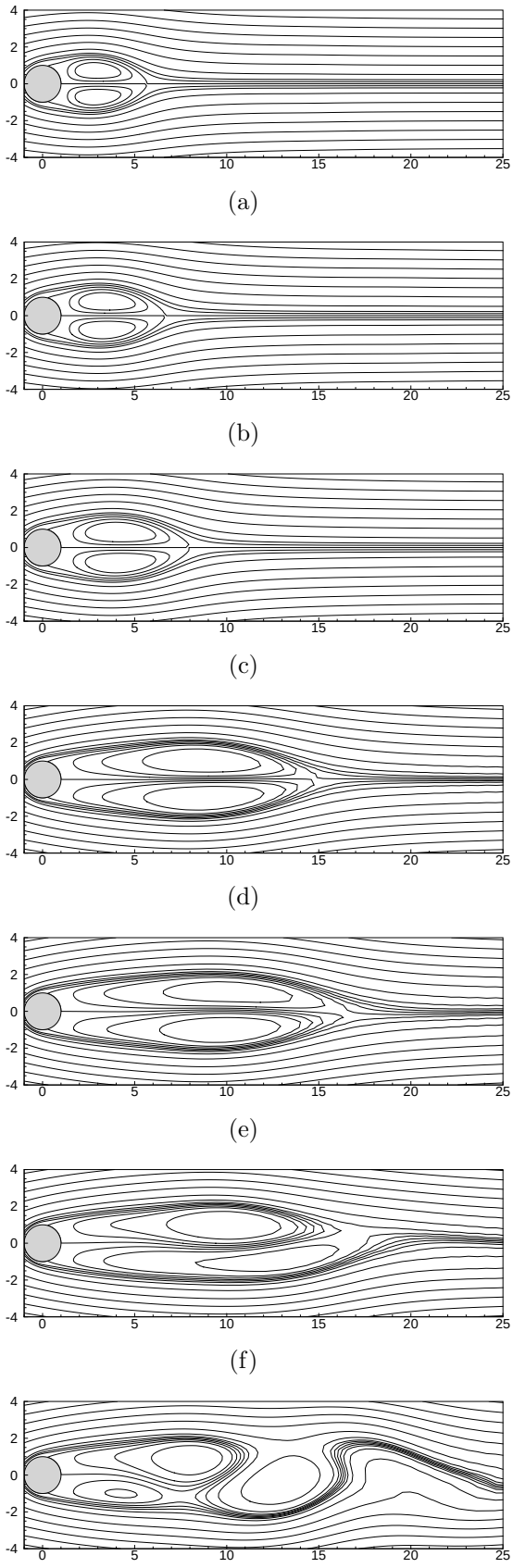

Figure 2: *Streamlines at $Re = 200$ for flow past a circular cylinder at: (a) $t = 15$, (b) $t = 20$, (c) $t = 28$, (d) $t = 84$, (e) $t = 100$ (f) $t = 110$, (g) $t = 126$, (h) $t = 146$, (i) $t = 313$, (j) $t = 413$.*

Here $0 \leq \lambda \leq 1$. For $\lambda = \frac{1}{2}$ we get $O(h^2, \delta t^2)$ implicit Crank-Nicolson type scheme. Here h is the uniform space length in the x and y-directions, δt is the uniform time step and (n), $(n+1)$ represent the time levels at the current and next time steps. The calculations are performed by time marching, using a predictor-corrector approach.

3 Results and Discussion

In order to resolve the quantitative and qualitative fluid flow features, we focus on a chosen Reynolds number value of 200 and consider far field $R_\infty \approx 43$. It is heartening to note that on a relatively coarser grid of size 181×301, we are able to accurately capture the characteristics of the flow including the von Kármán vortex street behind the cylinder.

In our computations, we used the uniform flow parameters as initial conditions and present the solution profiles in Fig. 2 for various values of t. As seen in Fig. 2, a symmetric flow was observed at the beginning (figure 2(a), 2(b), 2(c), 2(d)), but there is the initiation of the near-wake instability at a time around $t = 100$ (figure 2(e)) resulting in loss of symmetry. The wake starts oscillating transversely which is clearly visible in figure 2(f) and become unstable. Eventually, the flow settled into a periodic nature (figure 2(j)). We present the temporal

ISBN: 978-988-18210-8-9
ISSN: 2078-0958 (Print); ISSN: 2078-0966 (Online)

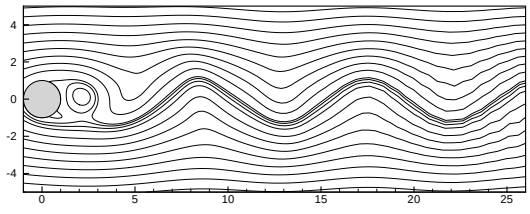

(a)

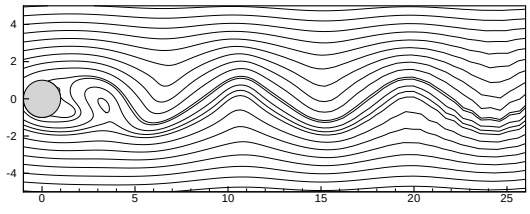

(b)

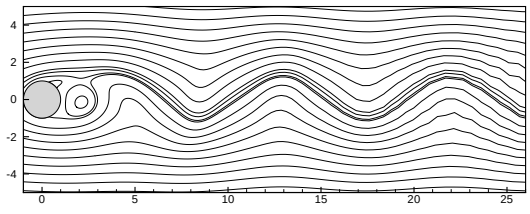

(c)

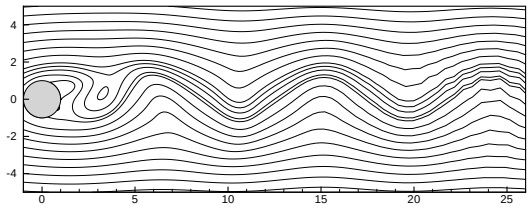

(d)

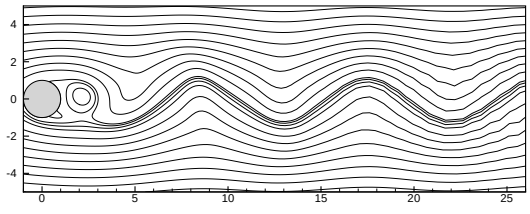

(e)

Figure 3: *The streamfunction contours depicting the wake behind the cylinder for five successive instants of time (a) $t = T$, (b) $t = T + \frac{T_0}{4}$, (c) $t = T + \frac{T_0}{2}$, (d) $t = T + \frac{3T_0}{4}$, (e) $t = T + T_0$*

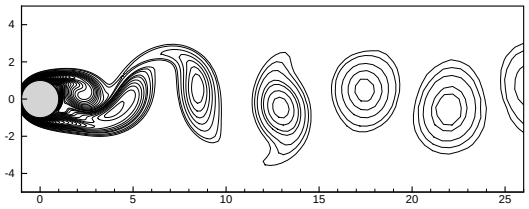

(a)

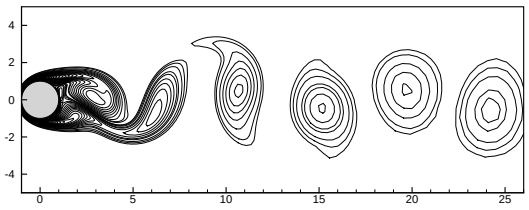

(b)

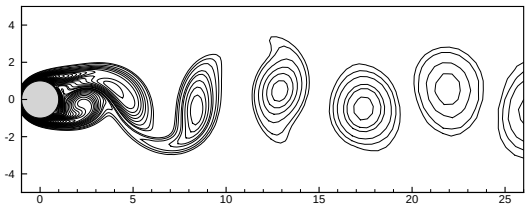

(c)

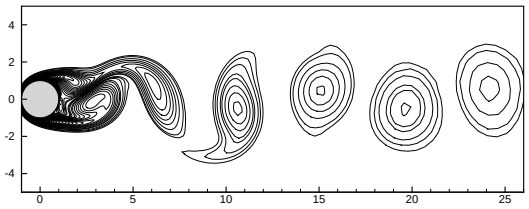

(d)

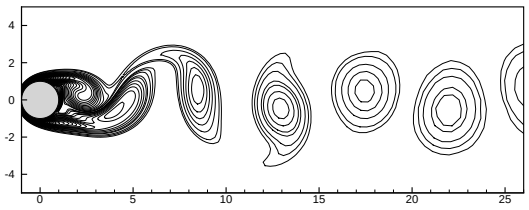

(e)

Figure 4: *The post processed vorticity contours for five successive instants of time (a) $t = T$, (b) $t = T + \frac{T_0}{4}$, (c) $t = T + \frac{T_0}{2}$, (d) $t = T + \frac{3T_0}{4}$, (e) $t = T + T_0$*

ISBN: 978-988-18210-8-9
ISSN: 2078-0958 (Print); ISSN: 2078-0966 (Online)

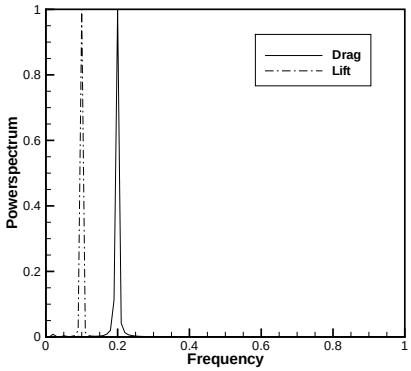

Figure 5: Periodic flow for $Re = 200$: Power spectra of the time series of the lift coefficient.

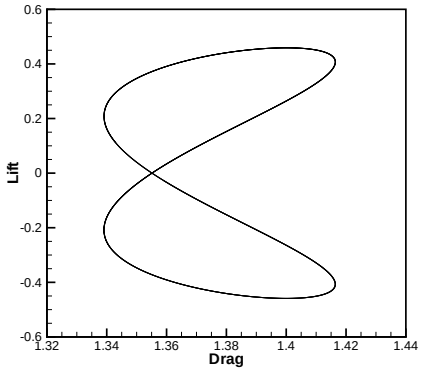

Figure 6: Periodic flow for $Re = 200$: Phase plane trajectories of Drag-Lift.

evolution of streamlines and post processed vorticity contours over one complete vortex shedding cycle of duration T in figure 3 and figure 4 respectively. The evolution of an impressive von Kármán vortex street, which is a regular feature of this flow for the Reynolds number considered here, is clearly seen in these figures. From Fig. 4, one can see the formation of eddies just behind the circular cylinder; these eddies are then washed away into the wake region. Two eddies are shed just behind the cylinder within each period. Figures 4(a) and 4(c) are half a vortex-shedding cycle apart, and hence figure 4(c) is a mirror image of Figures 4(a) and 4(e). The periodic nature of the sequence is also apparent from figures 3(a)-(e). The staggered nature of the Kármán shedding is clear from these plots. The crests and troughs of the sinuous waves in the streamlines reflect the alternatively positive and negative vorticities of the eddies. The power density spectra of this analysis is shown in Fig. 5. Fig. 6 displays the phase-plane of drag-lift for the same time sample. It clearly establishes the periodic nature of the flow for the Reynolds number considered and also the fact that the time period for one complete cycle for the lift coefficient is twice that of the drag coefficient. In Fig. 7, we show the time histories of the drag and lift coefficients which besides releaving the eventual periodic nature of the flow, also re-establishes the facts of Fig. 5 and Fig 6. In table 1, we compare the Strouhal number, drag and lift coefficients from our computations with established experimental and numerical results. In all the cases, our results are excellent match with them.

Table 1: *Comparison of Strouhal numbers, drag and lift coefficients of the periodic flow for* $Re = 200$.

Reference	St	C_D	C_L
Williamson (exp.) [12]	0.197		
Le *et al.* [13]	0.187	1.34 ± 0.030	±0.43
Linnick and Fasel [13]	0.197	1.34 ± 0.044	±0.69
Frank *et al.* [14]	0.194	1.31	± 0.65
Berthelsen and Faltinsen [13]	0.200	1.37± 0.046	± 0.70
Present Study	0.199	1.37 ± 0.038	±0.46

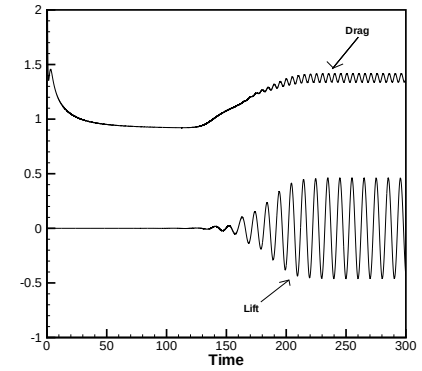

Figure 7: Evolution of drag and lift coefficients for the motion past a circular cylinder for $Re = 200$.

4 Conclusion

In this paper, we present the simulation of laminar flow past a circular cylinder by a recently developed implicit unconditionally stable biharmonic formulation for the unsteady two-dimensional Navier- Stokes equations. The robustness of the scheme is highlighted when it captures the von Kármán street behind the cylinder, clearly indicating that our scheme can accurately capture incompressible viscous flows on geometries beyond rectangular containing multiply-connected regions as well. Because of its high computational efficiency, our scheme has a good potential for efficient application to many more problems and our method is an important addition to the high accuracy solution procedures for transient incompressible viscous flows.

References

[1] Goldstein S, and Rosenhead L. Boundary layer growth. *Proc. Cad. Phil. Soc.*, 1936; **32**:392-401.

ISBN: 978-988-18210-8-9
ISSN: 2078-0958 (Print); ISSN: 2078-0966 (Online)

[2] Schuh H. Calculation of unsteady boundary layers in two dimensional laminar flow. *Z. Fluqwiss.*, 1953; **1**:122-133.

[3] Wundt H. Wachstum der laminaren Grenzschicht an schrag angestromten Zylindern bei Anfahrt aua der Ruhe. *Ing.-Arch. Berlin*, 1955; **23**:212.

[4] Watson EJ. Boundary layer growth. *Proc. R. Soc. Lond. (A)*, 1955; **231**:104-116.

[5] M. Coutanceau, R. Bouard, Experimental determination of the main features of the viscous flow in the wake of a circular cylinder in uniform translation. Part 1. Steady flow, *J. Fluid Mech.* 1977, **79**:231 - 256.

[6] M. Coutanceau, R. Bouard, Experimental determination of the main features of the viscous flow in the wake of a circular cylinder in uniform translation. Part 2. Unsteady flow, *J. Fluid Mech.* 1977, **79**: 257-272.

[7] R. Bouard, M. Coutanceau, The early stage of development of the wake behind an impulsively started cylinder for $40 < Re < 10^4$, *J. Fluid Mech.* 1980 **101(3)**:583-607.

[8] D.J. Tritton, Experiments on the flow past a circular cylinder at low Reynolds numbers, *J. Fluid Mech.* 1959 **6**: 547 - 567.

[9] C.H.K. Williamson, Oblique and parallel modes of vortex shedding in the wake of a circular cylinder at low Reynolds numbers, *J. Fluid Mech.* 1989 **206**: 579 - 627.

[10] C. Norberg, An experimental investigation of the flow around a circular cylinder: influence of aspect ratio, *J. Fluid Mech.* 1994 **258** : 287 - 316.

[11] C.A. Friehe, Vortex shedding from cylinders at low Reynolds numbers, *J. Fluid Mech.* 1980 **100**: 237 - 241.

[12] Williamson CHK. Oblique and parallel modes of vortex shedding in the wake of a circular cylinder at low Renolds numbers. *J. Fluid Mech.*, 1989; **206**:579–627.

[13] Berthelsen PA, Faltinsen OM. A local directional ghost cell approach for incompressible viscous flow problems with irregular boundaries. *J. Comput. Physics*, 2008; **227**:4354–4397.

[14] Franke R, Rodi W, Schonung B. Numerical calculation of laminar vortexshedding flow past cylinders. *Journal of Wind Engineering and Industrial Aerodynamics*, 1990; **35**: 237-257.

[15] Kalita JC and Ray RK, A transformation-free HOC scheme for incompressible viscous flows past an impulsively started circular cylinder, *Journal of Computational Physics* 2009 **228(14)**: 5207-5236.

[16] Mittal S and Raghuvanshi A., Control of vortex shedding behind circular cylinder for flows at low Reynolds numbers. *Int. J. Numer. Methods Fluids.*, 2001; **35**:421-447.

[17] Perry AE, Chong MS, Lim TT., The vortex shedding behind two-dimensional bluff bodies. *J. Fluid Mech.*, 1982; **116**:77 - 90.

[18] Gupta MM, Kalita JC., A new paradigm for solving NavierStokes equations: streamfunctionvelocity formulation. *J. Comput. Phys.*, 2005; **207**:52 - 68.

[19] Kupferman R., A central difference scheme for a pure streamfunction formulation of incompressible viscous flow. *SIAM J. Sci. Comput.*, 2001; **23**(1): 1 - 18.

[20] Fishelov D, Ben-Artzi M, Croisille JP., A compact scheme for the streamfunction formulation of Navier-Stokes equations. *Notes on Computer Sciences (Springer-Verlag)*, 2003; **2667**:809 - 817.

[21] Ben-Artzi M, Croisille JP, Fishelov D, Trachtenberg S., A pure-compact scheme for the streamfunction formulation of Navier-Stokes equations. *J. Comput. Phys.*, 2005; **205**(2):640–664.

[22] Gupta MM, Kalita JC., New paradigm continued: further computations with streamfunctionvelocity formulation for solving Navier-Stokes equations. *Communications in Applied Analysis*, 2006; **10**(4):461–490.

[23] Kalita JC., Gupta MM, A streamfunction-velocity approach for the 2D transient incompressible viscous flows. *Int. J. Numer. Meth. Fluids*, **62(3)** : 237-266, 2010.

[24] Kalita JC, Sen S., An efficient ψ-v formulation for transient incompressible viscous flows on irregular domains, **communicated**, *J. Comput. Phys.*.

ISBN: 978-988-18210-8-9
ISSN: 2078-0958 (Print); ISSN: 2078-0966 (Online)